Excitonic Bose-Einstein condensation in Ta₂NiSe₅ above room temperature

K. Seki,[1] Y. Wakisaka,[2] T. Kaneko,[1] T. Toriyama,[1] T. Konishi,[3] T. Sudayama,[2] N. L. Saini,[4] M. Arita,[5] H. Namatame,[5]
M. Taniguchi,[5,6] N. Katayama,[7] M. Nohara,[8] H. Takagi,[9] T. Mizokawa,[2] and Y. Ohta[1]

[1]*Department of Physics, Chiba University, Inage-ku, Chiba 263-8522, Japan*
[2]*Department of Physics and Department of Complex Science and Engineering, University of Tokyo, Kashiwa, Chiba 277-8561, Japan*
[3]*Department of Nanomaterial Science, Chiba University, Inage-ku, Chiba 263-8522, Japan*
[4]*Department of Physics, Sapienza University of Rome, 00185 Rome, Italy*
[5]*Hiroshima Synchrotron Radiation Center, Hiroshima University, Higashi-Hiroshima 739-0046, Japan*
[6]*Graduate School of Science, Hiroshima University, Higashi-Hiroshima 739-8526, Japan*
[7]*Department of Applied Physics, Nagoya University, Chikusa-ku, Nagoya 464-8601, Japan*
[8]*Department of Physics, Okayama University, Tsushima-naka, Okayama 700-8530, Japan*
[9]*Department of Physics, University of Tokyo, Bunkyo-ku, Tokyo 113-0033, Japan*

We show that finite temperature variational cluster approximation (VCA) calculations on an extended Falicov-Kimball model can reproduce angle-resolved photoemission spectroscopy (ARPES) results on Ta₂NiSe₅ across a semiconductor-to-semiconductor structural phase transition at 325 K. We demonstrate that the characteristic temperature dependence of the flat-top valence band observed by ARPES is reproduced by the VCA calculation on the realistic model for an excitonic insulator only when the strong excitonic fluctuation is taken into account. The present calculations indicate that Ta₂NiSe₅ falls in the Bose-Einstein condensation regime of the excitonic insulator state.

PACS number(s): 71.35.Lk, 67.85.Jk, 71.20.−b

I. INTRODUCTION

The diversity of Bose-Einstein condensation (BEC) with spin (and orbital) degrees of freedom is one of the main targets in the research of ultracold atom systems [1–3]. On the other hand, in electronic systems with holelike and electronlike Fermi pockets, interaction between hole and electron in the Fermi pockets tends to induce charge density wave (CDW) or spin density wave (SDW) with wave vector Q which spans the holelike and electronlike Fermi pockets in the Brillouin zone. Such CDW or SDW transitions can be described as Peierls transitions due to Fermi surface nesting. An alternative way to understand CDW or SDW transitions in the electronic systems is the theory for excitonic insulators that was proposed nearly half a century ago [4–7]. Since the electron and hole concentrations are relatively low, Coulomb interaction between holes and electrons in the Fermi pockets is weakly screened and stabilizes electron-hole bound states (excitons) with wave vector Q. In the Peierls picture and the excitonic insulator picture for metallic systems, the CDW or SDW transitions are basically BCS type. On the other hand, the theory of excitonic insulators can be extended to semiconductors where excitons are formed due to Coulomb interaction between valence band holes and conduction band electrons and undergo BEC. Very recently, BCS-BEC crossover of an excitonic insulator has been examined in more advanced calculations using such as a Mott-Wannier-type exciton model with T-matrix approximation [8] and an extended Falicov-Kimball model (EFKM) [9–11]. If the normal state above the excitonic transition temperature is semimetallic, namely the magnitude of the band gap $E_G < 0$, the excitonic transition is well described in the BCS framework. On the other hand, the excitonic transition is expected to be a BEC of excitons if the normal state is semiconducting or $E_G > 0$ as schematically shown in Fig. 1(a). In the BEC regime with $E_G > 0$, a

large amount of excitons are preformed above the excitonic transition temperature and the excitonic transition corresponds to the BEC of excitons.

The BEC transition temperature of excitons can be much higher than those of liquid He or cold atoms since the electron and hole masses are much smaller than atomic masses. Therefore, the BEC regime of the excitonic insulator can provide a unique opportunity to study "high temperature" BEC. Real materials studied in relevance to excitonic insulator states are limited to several rare-earth or transition-metal calcogenides such as Tm(Se,Te) [12,13] and 1T-TiSe₂ [14]. The possible excitonic insulator transition in Tm(Se,Te) has been studied using various transport measurements including electrical resistivity [12] and heat conductivity [13]. Although the increase of electrical resistivity at the transition and the increase of heat conductivity at the low temperature are assigned to the BEC and the superfluidity of excitons respectively, the excitonic insulator transition in Tm(Se,Te) is not established well due to the lack of quantitative theory. On the other hand, the CDW transition in semimetallic 1T-TiSe₂, which has holelike (electronlike) Fermi pockets at the zone center (boundary), has been identified as a BCS-like excitonic insulator transition by angle-resolved photoemission spectroscopy (ARPES) [14]. The BCS-like excitonic transition in 1T-TiSe₂ is a semimetal-to-semimetal transition due to the small off-stoichiometry or the small difference between the hole and electron densities. Therefore, it is rather difficult to characterize the excitonic transition by means of transport measurement, and the band dispersion observed by ARPES is the very direct evidence of the excitonic transition. The BCS-like excitonic transition can be described by the mean-field theory and the ARPES result can be compared with the theoretical calculation [14]. As for the BEC-like excitonic transition, it has been proposed that Ta₂NiSe₅ would have an excitonic insulator transition in the BEC regime based
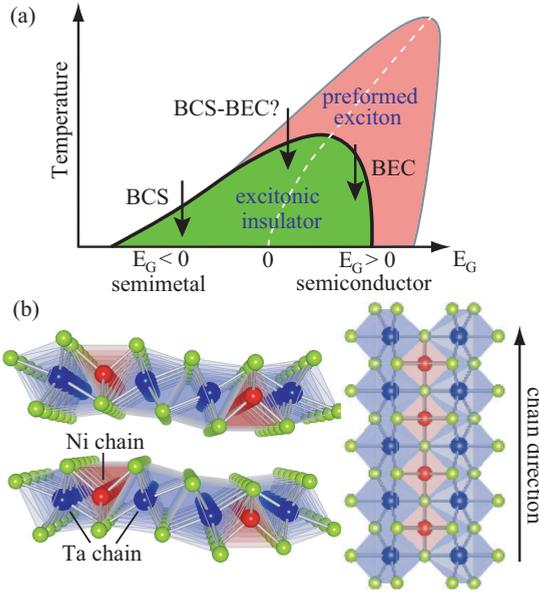
FIG. 1. (Color online) (a) Electronic phase diagram of an excitonic insulator as a function of temperature and band gap E_G. The white dashed curve indicates the boundary between semimetal and semiconductor regions, which roughly corresponds to the BCS-BEC crossover. In the BEC region, preformed excitons are formed even above the excitonic insulator transition temperature. (b) Sketch of quasi-1D crystal structure of Ta_2NiSe_5. The excitons are formed between the electrons at the Ta chains and the holes at the Ni chains.

on the ARPES results below the transition temperature [15]. The BEC-like excitonic transition is an insulator-insulator transition, and it is rather difficult to identify the BEC of excitons using transport measurement. Similar to the BCS-like excitonic transition in $1T$-TiSe$_2$, the band dispersion observed by ARPES can be one of the most straightforward evidence of the excitonic transition. Namely, the single particle excitation can be a fingerprint of the excitonic BEC just like the opening of a superconducting gap in the BEC of Cooper pairs. However, the BEC regime of the excitonic insulator transition cannot be described by the mean-field theory and, therefore, a new theory beyond mean-field approximation should be developed and compared with the ARPES result in order to establish the excitonic insulator transition in the BEC regime. In this sense, the BEC-like excitonic transition is not well established yet in any real materials including Ta_2NiSe_5.

As illustrated in Fig. 1(b), Ta_2NiSe_5 has a quasi-one-dimensional (quasi-1D) structure where Ni and Ta atoms are arranged in one-dimensional chains [16,17]. Resistivity of Ta_2NiSe_5 is insulating below 500 K and exhibits an anomaly around 325 K which is assigned as second-order or weak first-order structural phase transition without CDW. The resistivity exhibits insulating behaviors both above and below the transition temperature at 325 K. The magnetic susceptibility shows a gradual drop around 325 K suggesting spin singlet formation. The flattening and sharpening of the valence band top in insulating Ta_2NiSe_5 suggests that the phase transition at 325 K corresponds to an excitonic insulator transition in the BEC regime. In addition, Ta_2NiSe_5 is unique in that the excitons are formed between the electrons and holes

that are located in spatially separated chains, i.e., holes in the Ni chain and electrons in the two neighboring Ta chains in the quasi-1D structural units, which has an interesting similarity with the 2D bilayer electron systems of semiconductors where the electrons and holes are also spatially separated [18]. In the present work we have developed finite temperature variational cluster approximation (VCA) methods on EFKM for Ta_2NiSe_5 and have applied it to interpret temperature-dependent ARPES results of Ta_2NiSe_5 across the transition and to reveal the nature of the transition in this material.

II. EXTENDED FALICOV-KIMBALL MODEL

In order to include the electron correlation effects on the single-particle excitation spectra of Ta_2NiSe_5 across the excitonic insulator transition, we have employed VCA calculations on EFKM which is known as a minimal lattice model to describe the excitonic insulator state [9–11]. The Ta $5d$ and Ni $3d$ orbital degeneracy at the conduction-band bottom and the valence-band top is removed due to the quasi-one-dimensional structure [11]. Therefore, in order to describe the excitonic condensation and spectral function of valence-band top, the Coulomb interaction between the valence-band hole and the conduction-band electron is enough and, consequently, the EFKM with nondegenerate and spinless conduction and valence bands is sufficient. The Hamiltonian of the EFKM [9–11] is given as

$$\mathcal{H} = -\sum_{\delta=x,y,z} t_c^\delta \sum_{\langle ij \rangle} (c_i^\dagger c_j + \text{H.c.}) + (D/2 - \mu) \sum_i n_{ic}$$
$$- \sum_{\delta=x,y,z} t_f^\delta \sum_{\langle ij \rangle} (f_i^\dagger f_j + \text{H.c.}) + (-D/2 - \mu) \sum_i n_{if}$$
$$+ U \sum_i n_{ic} n_{if}, \tag{1}$$

where c_i ($c_i^\dagger$) denotes the annihilation (creation) operator of an electron on the c orbital (corresponding to the Ta $5d$ conduction band) at site i and $n_{ic} = c_i^\dagger c_i$ is the particle number operator. t_c^δ represents the spatially anisotropic hopping integral between neighboring sites parallel ($\delta = x$) and perpendicular ($\delta = y,z$) to the one-dimensional chain direction, as it is realized in the quasi-one-dimensional material Ta_2NiSe_5. These are the same for the f orbital (corresponding to the Ni $3d$-Se $4p$ valence band). D is the on-site energy split between the c and f orbitals and U is the interorbital Coulomb repulsion between electrons. Note that U can be considered as an interorbital electron-hole attraction and thus can drive the excitonic insulator state in this model at low temperature. The effect of the electron-lattice interaction has been examined in Ref. [19] and it has been found that the electron-lattice interaction plays a secondary role and helps the excitonic transition driven by the electron-hole interaction [19]. The chemical potential μ is determined so as to maintain the average particle density at half filling. The order parameter is given by

$$2\Delta = U\langle c_i^\dagger f_i + \text{H.c.} \rangle. \tag{2}$$

We use a parameter set of $t_c^x = -t_f^x = 0.4$ eV, $t_c^y = -t_f^y = -t_c^z = t_f^z = 0.024$ eV, $D/2 = 0.44$ eV, and $U = 0.84$ eV so as to reproduce the single-particle excitation spectrum observed

in ARPES for Ta_2NiSe_5 and the transition temperature at the same time. The dependence on the cluster size of the calculated results was checked by changing the cluster size such as the one-dimensional 4-, 5-, 6-site (8-, 10-, and 12-orbital) clusters, where each site contains a pair of the c and f orbitals, and no significant cluster-size dependence was found. Here it should be noted that this parameter set corresponds to the semimetallic state in the noninteracting ($U = 0$) limit while it can describe the semiconducting state due to the Hartree shift by U [10].

III. METHODS

A. Variational cluster approximation

The VCA [20] with its finite temperature algorithm was employed to calculate the temperature dependence of the excitonic order parameter and the single-particle excitation spectra. Here let us describe the formulation of the variational cluster approximation (VCA) at finite temperature used in this article.

First we briefly review the rigorous variational principle for the thermodynamic potential functional derived by Luttinger and Ward [21] and revisited by Potthof [20]. It has been shown by Potthoff [20] that the thermodynamic potential functional as a functional of the self-energy can be written as

$$\Omega[\mathbf{\Sigma}] = \mathcal{F}[\mathbf{\Sigma}] - \mathrm{Tr} \ln \left(-\mathbf{G}_0^{-1} + \mathbf{\Sigma}\right), \quad (3)$$

where $\mathcal{F}[\mathbf{\Sigma}]$ is the Legendre transform of the Luttinger-Ward functional $\Phi[\mathbf{G}]$ [21], $\mathbf{G}_0$ is the noninteracting Green's function, and the self-energy $\mathbf{\Sigma}$ is considered as a trial function for the variational calculation described below. Tr represents the sum over fermionic Matsubara frequencies $i\omega_\nu = (2\nu + 1)\pi T$, where T is the temperature and ν is an integer, and trace over the single-particle basis. The stationarity condition

$$\delta\Omega[\mathbf{\Sigma}]/\delta\mathbf{\Sigma} = 0 \quad (4)$$

gives the Dyson equation and the functional at the stationary point gives the thermodynamic potential of the system [20,21].

The self-energy functional theory (SFT) [20] provides a way to compute Ω by using the fact that the functional form of $\mathcal{F}[\mathbf{\Sigma}]$ depends only on the interaction terms of the Hamiltonian. In SFT, the original lattice is divided into disconnected finite-size clusters and the reference system is introduced as their collection. The clusters form a superlattice and have the same interaction term as the original system because the interaction term of the Hamiltonian of the extended Falicov-Kimball model [EFKM, Eq. (1)] is local in real space. Therefore, the functional form $\mathcal{F}[\mathbf{\Sigma}]$ of the reference system is the same for that of the original system. The exact thermodynamic potential of the reference system is given by $\Omega' = \mathcal{F}[\mathbf{\Sigma}'] - \mathrm{Tr} \ln(-\mathbf{G}_0'^{-1} + \mathbf{\Sigma}')$, where $\mathbf{G}_0'$ and $\mathbf{\Sigma}'$ are the noninteracting Green's function and the exact self-energy of the reference system, respectively. Then, by restricting the self-energy $\mathbf{\Sigma}$ to $\mathbf{\Sigma}'$, we can eliminate the functional $\mathcal{F}[\mathbf{\Sigma}']$ and obtain

$$\Omega[\mathbf{\Sigma}'] = \Omega' - \mathrm{Tr} \ln(\mathbf{I} - \mathbf{V}\mathbf{G}'), \quad (5)$$

where $\mathbf{I}$ is the unit matrix, $\mathbf{V} \equiv \mathbf{G}_0'^{-1} - \mathbf{G}_0^{-1}$ represents the difference of the one-body terms between the original

and reference systems, and $\mathbf{G}' = (\mathbf{G}_0'^{-1} - \mathbf{\Sigma}')^{-1}$ is the exact Green's function of the reference system. The size of these matrices are $2L_c \times 2L_c$, where L_c is the number of sites within a disconnected finite-size cluster.

The Hamiltonian of the reference system is defined as

$$\mathcal{H}' = \mathcal{H} + \mathcal{H}_{\mathrm{EI}}, \quad (6)$$

$$\mathcal{H}_{\mathrm{EI}} = \Delta' \sum_i (c_i^\dagger f_i + \mathrm{H.c.}), \quad (7)$$

where $\mathcal{H}$ is the Hamiltonian of the EFKM defined in Eq. (1), and Δ' is a Weiss field for excitonic condensation which is treated as a variational parameter. In other words, the self-energy $\mathbf{\Sigma}$ is varied through Δ' and thus the variational principle Eq. (4) is practically given by $\partial\Omega/\partial\Delta' = 0$. Note that the solution with $\Delta' \neq 0$ corresponds to the spontaneous EI state. Then we solve the eigenvalue problem $\mathcal{H}'|\Psi_n\rangle = E_n|\Psi_n\rangle$ for all excited states of a finite-size cluster and calculate the trial single-particle Green's function. The Green's function matrix in Eq. (5) is defined as

$$\mathbf{G}'(\omega) = \begin{pmatrix} \mathbf{G}'^{cc}(\omega) & \mathbf{G}'^{cf}(\omega) \\ \mathbf{G}'^{fc}(\omega) & \mathbf{G}'^{ff}(\omega) \end{pmatrix}, \quad (8)$$

with the matrix elements of

$$G_{ij}'^{cf}(i\omega_\nu) = e^{\beta\Omega'} \sum_{r,s} (e^{-\beta E_r} + e^{-\beta E_s}) \frac{\langle \Psi_r | c_i^\dagger | \Psi_s \rangle \langle \Psi_s | f_j | \Psi_r \rangle}{i\omega_\nu - (E_r - E_s)}, \quad (9)$$

where $|\Psi_r\rangle$ is an eigenstate of $\mathcal{H}'$ and E_r is the corresponding eigenvalue.

B. Cluster perturbation theory

The single-particle excitation spectra are calculated by the cluster perturbation theory (CPT) [22]. In the CPT, the single-particle Green's function is given as

$$\mathcal{G}^\alpha(\mathbf{k},\omega) = \frac{1}{L_c} \sum_{i,j}^{L_c} G_{\mathrm{CPT},ij}^\alpha(\mathbf{k},\omega) e^{-i\mathbf{k}\cdot(\mathbf{r}_i - \mathbf{r}_j)}, \quad (10)$$

where α ($=c,f$) denotes the orbital index, $\mathbf{r}_i$ is the position of the ith site within a cluster, and

$$\mathbf{G}_{\mathrm{CPT}}^\alpha(\mathbf{k},\omega) = \{\mathbf{G}'(\omega)[\mathbf{I} - \mathbf{V}(\mathbf{k})\mathbf{G}'(\omega)]^{-1}\}^{\alpha\alpha} \quad (11)$$

is the CPT Green's function [22]. Note that the wave vector $\mathbf{k}$ can take arbitrary values in the Brillouin zone. The CPT is exact both in the noninteracting ($U = 0$) and atomic ($t = 0$) limits, and is expected to work well in the strongly interacting regime since it is derived originally from the strong-coupling expansion for the single-particle Green's function. In the weak-to intermediate-coupling regime, the CPT approximation is generally improved with increasing the cluster size [22]. Thus larger clusters are in principle required to obtain more accurate results. We have checked calculations of single-particle excitation spectra as well as the excitonic order parameters for one-dimensional clusters of the size $L_c = 4, 5,$ and 6 (8, 10, and 12 orbital), where each site contains a pair of the c and f orbitals, and have found no significant cluster-size dependence. In the next section, calculated results

for the $L_c = 5$ (10-orbital) cluster are shown, thus the effects of statical and dynamical electron correlation within the cluster size are taken into account.

C. Angle-resolved photoemission spectroscopy

The ARPES data compared to the calculated results were taken at beamline 9A, Hiroshima Synchrotron Radiation Center (HSRC) using a Scienta R4000 analyzer with an angular resolution of $\sim 0.3°$ and energy resolution ~ 26 meV using circularly polarized light of photon energy $h\nu = 23$ eV. The ARPES data with higher quality than those reported in Ref. [15] cover the temperature range from 40 to 360 K including the transition temperature ~ 325 K. The ARPES data partially reported in Ref. 20 [20] were reanalyzed considering the calculated results and are presented. ARPES spectra are obtained as $\rho_k(E)$, where E and k are electron energy and wave vector. In the second derivative plot, $-d^2\rho_k(E)/dE^2$ is smoothed and is plotted as a function of electron energy and wave vector.

IV. RESULTS AND DISCUSSION

A. Transport properties

Figure 2 shows the electrical resistivity ρ and $-T^2 d \ln\rho/dT$ as a function of temperature T as well as the magnetic susceptibility M/H of Ta_2NiSe_5. The electrical resistivity ρ and $-T^2 d \ln\rho/dT$ of Ta_2NiSe_5 exhibit an anomaly at 325 K which corresponds to the excitonic insulator transition. The resistivity exhibits insulating behaviors both
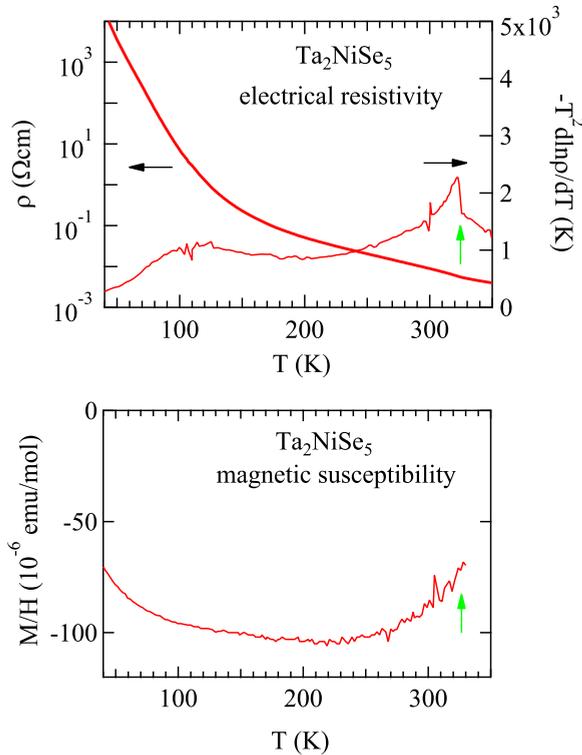
FIG. 2. (Color online) Electrical resistivity and magnetic susceptibility of Ta_2NiSe_5 as functions of temperature. The arrows indicate the transition temperature.

above and below the transition. If temperature dependence of resistivity is given by a simple activation type function $e^{E_G/k_B T}$ with band gap of E_G, ρ and $-T^2 d \ln\rho/dT$ provides magnitude of E_G/k_B. E_G is estimated to be ~ 1000 K which is consistent with the magnitude of the gap observed by ARPES. The magnetic susceptibility shows a gradual drop around 325 K which can be assigned to the gradual increase of the band gap due to the excitonic coupling between the valence band hole and the conduction band electron.

B. Temperature dependence of ARPES spectra

Figure 3 shows temperature dependence of ARPES spectra around the Γ point. In order to capture the temperature evolution of the band dispersions, the valence-band-peak positions evaluated from the energy distribution curves (which are indicated by the dots with the error bars in Fig. 3) were fitted to the model function $\epsilon_v(k)$ for the excitonic insulator band dispersion (shown by the thick solid curves in Fig. 3). The model function $\epsilon_v(k)$ for the excitonic insulator band dispersion is obtained as below:

$$\epsilon_v^0(k) = \epsilon_1 + \sqrt{(\epsilon_2/2)^2 + (2t_{Ni-Se}\cos^2 ka/2)^2}, \quad (12)$$

$$\epsilon_c^0(k) = \epsilon_3 - 2t_{Ta}\cos ka, \quad (13)$$

$$\epsilon_v(k) = \frac{\epsilon_v^0(k) + \epsilon_c^0(k)}{2} - \sqrt{\left(\frac{\epsilon_v^0(k) - \epsilon_c^0(k)}{2}\right)^2 + \Delta^2}. \quad (14)$$

Here $\epsilon_v^0(k)$ and $\epsilon_c^0(k)$ are the bare valence and conduction bands derived by a tight-binding model free from excitonic interaction. In the tight-binding model, the Ni-Se and Ta chains are considered to form one-dimensional band dispersion along the chain direction only through their nearest neighbor transfer integrals t_{Ni-Se} and t_{Ta} without interchain hybridization. Assuming linear temperature dependence of the chemical potential, the model function $\epsilon_v(k)$ is fitted to the valence-band-peak positions to optimize t_{Ni-Se} and the excitonic insulator order parameter Δ as adjustable parameters. The fitting results are shown by the thick solid curves in Fig. 3, indicating that the fits are reasonably good to extract Δ as a function of temperature. The bare valence-band dispersion $\epsilon_v^0(k)$ without the excitonic coupling is indicated by the thin solid curves in Fig. 3.

C. Comparison between VCA calculations and ARPES results

Overall valence-band dispersions observed by ARPES are consistent with the tight-binding or LDA band structure calculations [19,24]. However, there is a prominent discrepancy near the top of the valence band located at the Γ point where characteristically flat band dispersion is observed as shown in Fig. 4(a). This flat band dispersion reminds the experimental ARPES result of $1T$-$TiSe_2$, which is one of the candidate materials for showing excitonic insulator transition [14,25,26]. The experimentally observed bands of $1T$-$TiSe_2$ reported in the ARPES measurement [14] are well reproduced by BCS-like theoretical calculation assuming the excitonic insulator transition to be the origin of its CDW transition [25,26]. Paying attention to this similarity with
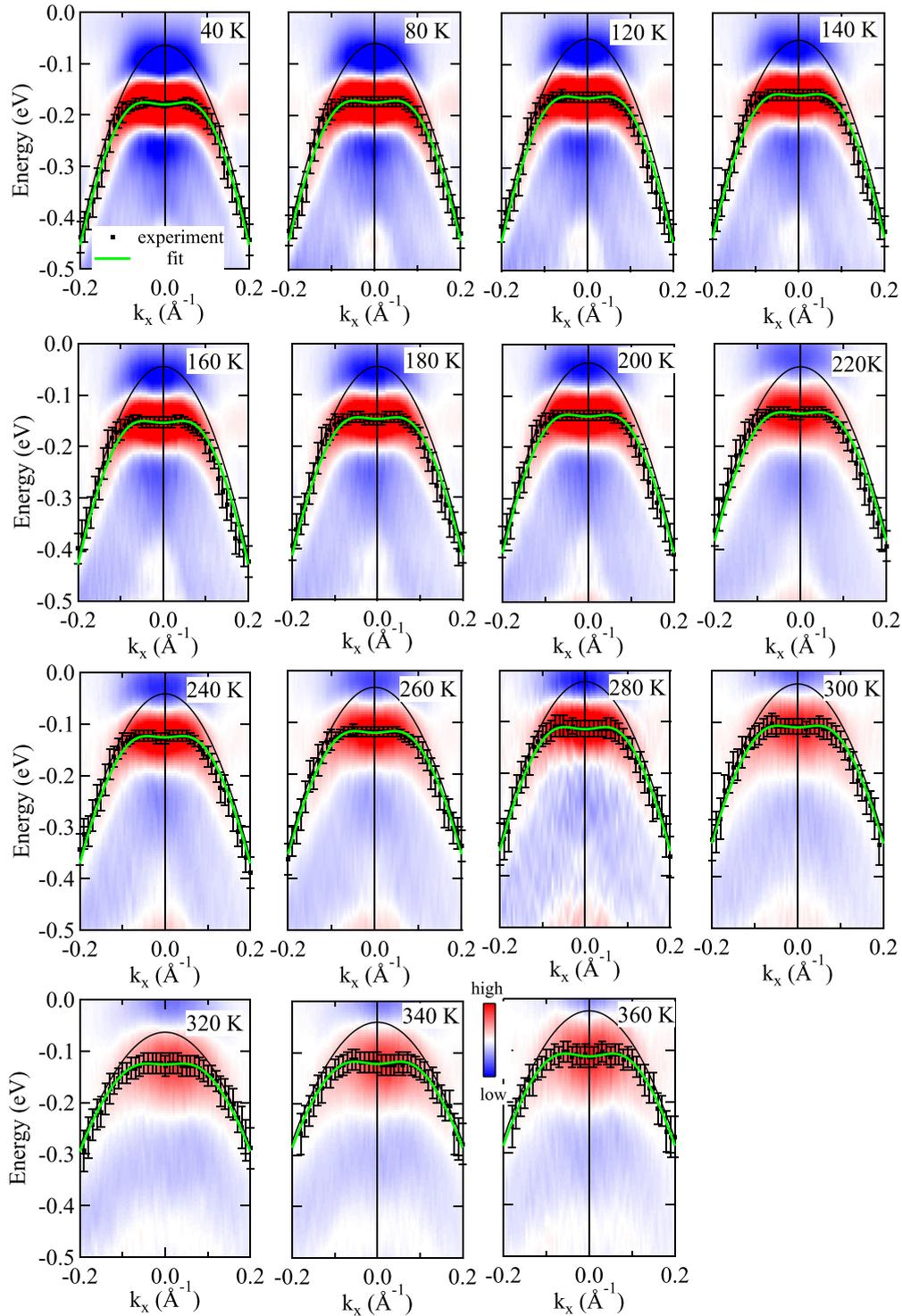
FIG. 3. (Color online) Second derivative plots of the ARPES spectra along the chain direction of Ta$_2$NiSe$_5$ taken at various temperatures. The valence-band-peak positions evaluated from the energy distribution curves are indicated by the dots with the error bars. The fit to the excitonic insulator band dispersion is shown by the thick solid curve. The thin solid curve indicates the bare valence-band dispersion without the excitonic coupling.

1T-TiSe$_2$, the ground state of Ta$_2$NiSe$_5$ can be viewed as an excitonic insulator state, in which Ni 3d-Se 4p valence band and Ta 5d conduction band hybridize each other due to electron-hole Coulomb interaction [15]. In order to discuss the nature of the transition to the excitonic insulator state,

we now analyze the temperature-dependent ARPES results across the transition [23] on the basis of finite temperature VCA calculations on EFKM.

Figure 4(b) shows temperature dependence in the second derivative plots of the ARPES energy distribution curves along
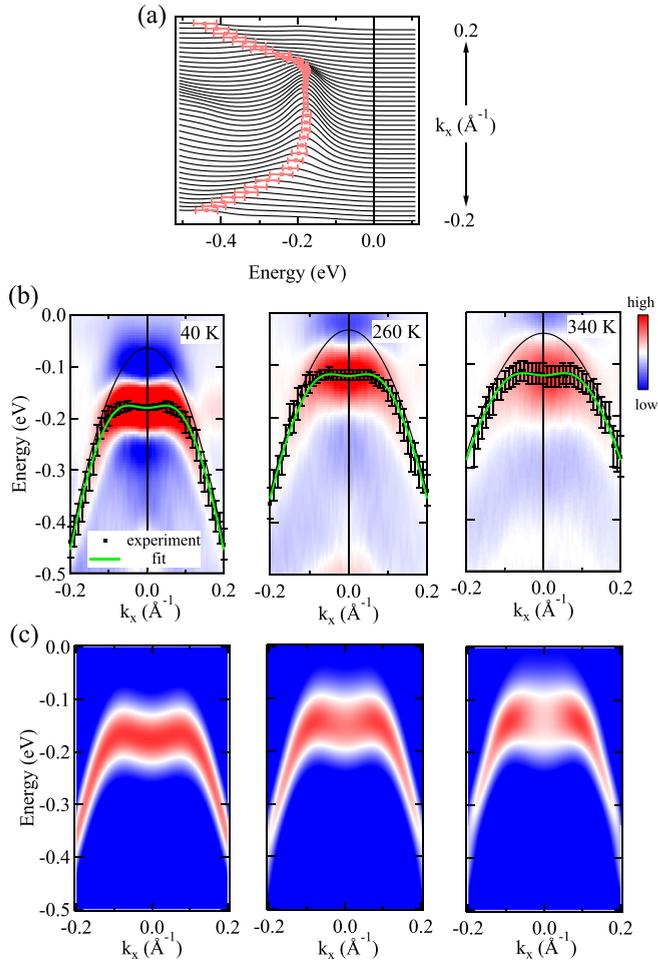
FIG. 4. (Color online) (a) Second derivative plots of the ARPES spectra along the Γ-X direction taken at 40 K. The specific flat band is formed at the top of valence band. (b) Band dispersions obtained from the ARPES spectra at 40, 260, and 340 K. The dots with error bars indicate the band positions determined from the ARPES data. The fit to the excitonic insulator band dispersion is shown by the thick solid curve. The thin solid curve indicates the bare valence-band dispersion without the excitonic coupling. (c) Single-particle excitation spectra for 40, 270, and 340 K obtained by the VCA calculation.

FIG. 5. (Color online) (a) ARPES spectra at Γ point taken at 40, 260, and 340 K, and single-particle excitation spectra at Γ point calculated for 40, 270, and 340 K and multiplied by the Fermi-Dirac distribution function. (b) Temperature dependencies of the peak position of the flat valence band at Γ (Δ_Γ) and the order parameter Δ, which are extracted from the ARPES results and are obtained from the VCA calculations.

the Ta and Ni chain directions. The second derivative plots at 40, 260, and 340 K are compared with the single-particle spectral function obtained by the VCA calculations on EFKM for 40, 270, and 340 K which are displayed in Fig. 4(c). The flat-top valence band at 40 K is well reproduced by the calculation on the EFKM with the appropriate parameter set as well as the previous mean-field calculation on the multiband Hubbard model [19]. Experimentally, as the temperature increases, the area of the flat band region in the momentum space decreases and the band top becomes closer to the Fermi level (E_F). The band dispersion deviates from the parabolic behavior and the flattening of the band top still remains even at 340 K, which is above the transition temperature. This situation is well explained by the present VCA calculation including the correlation effect beyond the mean-field or BCS limit. Here it should be noted that the flat band dispersion at 40 K exhibits a

dip at the Γ point which is explained by the VCA calculation on the quasi-1D EFKM.

By fitting the band positions to the band dispersion renormalized in a mean-field treatment assuming the excitonic insulator order parameter as indicated in Fig. 4, one can decompose the temperature dependence of the band top energy into the temperature dependence of Δ (due to the electron-hole interaction) and the temperature dependence of the bare valence band. The energy distribution curves (EDCs) of the Γ point at 40, 260, and 340 K (from which the temperature dependence of the bare valence band is subtracted) are compared with the calculated spectra for 40, 270, and 340 K in Fig. 5(a). As the temperature increases, the EDC peak position is shifted towards lower binding energy and the EDC peak width of the flat band becomes broader. The substantial spectral broadening is reminiscent of the breaking of the quasiparticle peak structure, namely, the breaking of the BEC. The broadening is similar to that observed in the pseudogap region of the high T_c cuprates although the cuprate case is more complicated with the pseudogap assigned to a possible competing order instead of the fluctuation of Cooper pairs [27]. Figure 5(b) shows the temperature dependence of the order parameter Δ and Δ_Γ (the energy position of the spectral peak relative to E_F at the Γ point) obtained from

the calculation. First, the value of $2\Delta/k_B T_c$ is approximately 10 indicating that the present transition falls in the strong coupling regime. Second, Δ_Γ remains finite even above the phase transition temperature as observed in the experiment showing that $E_G > 0$ due to the Hartree shift by U. Third, the band flattening remains even above the transition temperature indicating the excitonic fluctuation. Interestingly, the strong coupling nature and the strong fluctuation above the transition in Ta_2NiSe_5 are very similar to the recent ARPES observation on the strong coupling superconductivity with a pseudogap behavior in $FeSe_xTe_{1-x}$ [28]. The exciton fluctuation above the phase transition temperature is even indicated in a semimetal $1T$-$TiSe_2$ system which is thought to fall in the BCS regime of the phase diagram [29,30]. The present VCA calculation with fluctuation effect shows that the preformed exciton region in the conventional phase diagram [Fig. 1(a)] corresponds to the pseudogap phase with strong excitonic fluctuation. In addition, the transition-metal $5d$ or rare-earth $4f$ orbitals with spin and orbital degrees freedom under strong spin-orbit interaction can provide a variety of spin-orbit coupled condensates derived from their band gap structures and spin-orbital dependent Coulomb interactions. Therefore, the excitonic insulators including Ta_2NiSe_5 will provide a new playground to explore physics of BCS-BEC crossover in various bosonic systems with spin and orbital degrees freedom which have been attracting great interest due to the discoveries in the ultracold atom systems [1–3].

V. CONCLUSION

In summary, the transition to the excitonic insulator state in Ta_2NiSe_5 has been identified as a BEC of excitons based on the comparison between the finite temperature VCA calculations and the ARPES results. A flat dispersion around the top of the valence band was observed and assigned as the effect of excitonic coupling between the valence and conduction bands. As the system exceeds the transition temperature, the flat feature of the valence band weakens though the exciton fluctuations remain finite which is due to the strong fluctuation effect expected in the BEC character of the excitonic insulator transition from the semiconductor phase.

[1] C. Wang, C. Gao, C.-M. Jian, and H. Zhai, Phys. Rev. Lett. **105**, 160403 (2010).

[2] Y.-J. Lin, K. Jimenez-Garcia, and I. B. Spielman, Nature (London) **471**, 83 (2011).

[3] T.-L. Ho and S. Zhang, Phys. Rev. Lett. **107**, 150403 (2011).

[4] N. F. Mott, Philos. Mag. **6**, 287 (1961).

[5] D. Jérome, T. M. Rice, and W. Kohn, Phys. Rev. **158**, 462 (1967).

[6] J. Zittartz, Phys. Rev. **162**, 752 (1967).

[7] B. I. Halperin and T. M. Rice, Rev. Mod. Phys. **40**, 755 (1968).

[8] F. X. Bronold and H. Fehske, Phys. Rev. B **74**, 165107 (2006).

[9] D. Ihle, M. Pfafferott, E. Burovski, F. X. Bronold, and H. Fehske, Phys. Rev. B **78**, 193103 (2008).

[10] V.-N. Phan, K. W. Becker, and H. Fehske, Phys. Rev. B **81**, 205117 (2010).

[11] K. Seki, R. Eder, and Y. Ohta, Phys. Rev. B **84**, 245106 (2011).

[12] J. Neuenschwander and P. Wachter, Phys. Rev. B **41**, 12693 (1990).

[13] P. Wachter, B. Bucher, and J. Malar, Phys. Rev. B **69**, 094502 (2004).

[14] H. Cercellier, C. Monney, F. Clerc, C. Battaglia, L. Despont, M. G. Garnier, H. Beck, P. Aebi, L. Patthey, H. Berger, and L. Forró, Phys. Rev. Lett. **99**, 146403 (2007).

[15] Y. Wakisaka, T. Sudayama, K. Takubo, T. Mizokawa, M. Arita, H. Namatame, M. Taniguchi, N. Katayama, M. Nohara, and H. Takagi, Phys. Rev. Lett. **103**, 026402 (2009).

[16] S. A. Sunshine and J. A. Ibers, Inorg. Chem. **24**, 3611 (1985).

[17] F. J. DiSalvo, C. H. Chen, R. M. Fleming, J. V. Waszczak, R. G. Dunn, S. A. Sunshine, and J. A. Ibers, J. Less-Common Met. **116**, 51 (1986).

[18] J. P. Eisenstein and A. H. MacDonald, Nature (London) **432**, 691 (2004).

[19] T. Kaneko, T. Toriyama, T. Konishi, and Y. Ohta, Phys. Rev. B **87**, 035121 (2013); **87**, 199902(E) (2013).

[20] M. Potthoff, Eur. Phys. J. B **32**, 429 (2003); **36**, 335 (2003).

[21] J. M. Luttinger and J. C. Ward, Phys. Rev. **118**, 1417 (1960).

[22] D. Sénéchal, D. Perez, and M. Pioro-Ladriere, Phys. Rev. Lett. **84**, 522 (2000).

[23] Y. Wakisaka, T. Sudayama, K. Takubo, T. Mizokawa, N. L. Saini, M. Arita, H. Namatame, M. Taniguchi, N. Katayama, M. Nohara, and H. Takagi, J. Supercond. Nov. Magn. **25**, 1231 (2012).

[24] E. Canadell and M.-H. Whangbo, Inorg. Chem. **26**, 3974 (1987).

[25] C. Monney, H. Cercellier, F. Clerc, C. Battaglia, E. F. Schwier, C. Didiot, M. G. Garnier, H. Beck, P. Aebi, H. Berger, L. Forro, and L. Patthey, Phys. Rev. B **79**, 045116 (2009).

[26] C. Monney, E. F. Schwier, M. G. Garnier, N. Mariotti, C. Didiot, H. Beck, P. Aebi, H. Cercellier, J. Marcus, C. Battaglia, H. Berger, and A. N. Titov, Phys. Rev. B **81**, 155104 (2010).

[27] T. Kondo, A. D. Palczewski, Y. Hamaya, T. Takeuchi, J. S. Wen, Z. J. Xu, G. Gu, and A. Kaminski, Phys. Rev. Lett. **111**, 157003 (2013).

[28] Y. Lubashevsky, E. Lahoud, K. Chashka, D. Podolsky, and A. Kanigel, Nat. Phys. **8**, 309 (2012).

[29] C. Monney, G. Monney, P. Aebi, and H. Beck, Phys. Rev. B **85**, 235150 (2012).

[30] C. Monney, G. Monney, P. Aebi, and H. Beck, New J. Phys. **14**, 075026 (2012).